Low-energy electron scattering by tetrahydrofuran

A. Gauf, L. R. Hargreaves, A. Jo, J. Tanner, M. A. Khakoo, T. Walls, C. Winstead, and V. McKoy

Phys. Rev. A **85**, 052717 — Published 29 May 2012

DOI: 10.1103/PhysRevA.85.052717

Low-Energy Electron Scattering by Tetrahydrofuran

A. Gauf, L. R. Hargreaves, A. Jo, J. Tanner, and M. A. Khakoo

Department of Physics, California State University, Fullerton, California 92834, USA

T. Walls

Science Department, California High School,

9800 South Mills Avenue, Whittier, California 90604, USA

C. Winstead and V. McKoy

A. A. Noyes Laboratory of Chemical Physics,

California Institute of Technology, Pasadena, California 91125, USA

Abstract

Cross sections for elastic scattering of low-energy electrons by tetrahydrofuran, a prototype for the furanose ring found in the backbone of DNA, have been measured and calculated over a wide energy range, with an emphasis on energies below 6 eV, where previous data are scarce. The measurements employ a thin-aperture version of the relative-flow method, while the calculations employ the Schwinger multichannel method with an extensive treatment of polarization effects. Comparisons with earlier results, both experimental and theoretical, are presented and discussed. A proper accounting for the strong permanent electric dipole of tetrahydrofuran is found to be essential to obtaining reliable cross sections, especially at energies below 5 eV.

PACS numbers: 34.80.Bm, 34.80.Gs

I. INTRODUCTION

Since the demonstration by Sanche and coworkers [1, 2] that low-energy electrons can induce DNA strand breaks, there has been considerable attention paid to electron collision processes involving constituents of DNA. In particular, low-energy electron interactions with tetrahydrofuran (THF), the simplest model of the furanose ring that links the phosphate groups in the DNA backbone, have been studied intensively by both experimental [3–23] and computational [21, 24–28] methods. These studies have provided valuable information about processes relevant to understanding electron transport and reactivity in biological media, including vibrational [4, 8, 11, 15, 18] and electronic excitation [3, 8, 11, 20, 22, 23], dissocative attachment [5, 6, 10, 14, 19], electron trapping and reactivity in condensed THF [7, 11, 13], and the elastic [8, 15–17, 20] and total scattering [9, 12, 21] cross sections. Although the reported measurements of the elastic electron cross section are generally consistent, there are some disagreements at higher energies; more importantly, data below 6 eV collision energy are scant, with the only reported measurements being those of Allan [15]. Likewise, existing calculations of the elastic cross section are in fair to good agreement with each other and with experiment but do not cover the low-energy region well; in particular, our own previous calculations [27] did not account for long-range scattering by the significant static electric dipole moment of THF and were thus increasingly unreliable below about 5 eV.

In the present work, we have carried out measurements of the differential cross section (DCS) for elastic scattering of electrons by THF at energies as low as 0.75 eV, as well as calculations that incorporate both dipole-scattering corrections and a more extensive treatment of target polarization effects than in previous work.

II. METHOD

A. Experimental

The experimental apparatus has been described in previous articles, *e.g.,* Khakoo *et al.* [29]. The electron gun and the detector both employ double hemispherical energy selectors, and the apparatus is made of titanium. The spectrometer is heated by biaxial tantalum wire heaters to about 120° C to promote stability against contamination by the target gas or diffusion pump oil. The analyzer detector was a discrete dynode electron multiplier with

TABLE I: Molecular diameters, δ, determined from gas flow rate vs. drive pressure measurements. See Ref. [31] for details.

Gas	Mass (amu)	δ (10^{-8} cm, $\pm$7%)
H_2	2.02	2.74
N_2	28.02	3.75
C_2H_4	28.03	4.95
Furan	68.07	5.24
CH_3OH	32.04	6.30
H_2O	18.02	7.06
C_2H_5OH	46.07	7.15
iso-C_3H_7OH	60.11	7.35
n-C_3H_7OH	60.11	7.46
C_4H_8O (THF)	72.11	7.57
C_4H_8O (EVE)	72.11	7.84
n-C_4H_9OH	74.12	8.23

an extremely low background rate of <0.01 Hz and the capability of linearly detecting up to 1 MHz of electrons without saturating. The remnant magnetic field in the collision region is reduced to <1 mG by using a double μ-metal shield as well as a Hemholtz coil that eliminates the vertical component of the Earth's magnetic field. Typical electron currents were around 20 to 30 nA, with an energy resolution of 60 to 80 meV, full width at half maximum (FWHM). The large current was desirable to speed up data acquisition time and to obtain favorable scattered-electron count rates at higher incident electron energies E_0. The electron beam was stable to within 20%, requiring minor tuning of the spectrometer to maintain its long-term stability. The contact potential was determined before each daily set of runs by monitoring the $2\,^2$S He resonance at 19.366 eV [30], and we were able to calibrate our E_0 values to an uncertainty of $\pm$30 meV.

Elastic and vibrational energy-loss spectral peaks were measured at fixed E_0 values and electron scattering angles θ by repetitive, multichannel-scaling techniques. The THF spectra had a vibrational excitation feature lying close to the elastic peak, made up of several ring bend modes, two C–C stretch modes, and a CH_2 bend mode within a broad line profile

[4, 15] that has a width of about 100 meV FWHM centered nominally at about 0.15 eV. This feature was satisfactorily unfolded from the elastic line by fitting it to a Gaussian profile. Typically this vibrational feature was about 5 to 10% as strong as the elastic peak, but for large θ and for E_0=10 eV and above, it rose to almost 30% of the elastic in many instances. The angular resolution of the spectrometer was 2° FWHM. The electron detector (analyzer) was equipped with a 5-element zoom lens plus a virtual aperture system that made it possible to detect low energy electrons. The effusive target gas beam was formed by flowing gas through a thin aperture source 0.3 mm in diameter, described previously [31]. This aperture system was covered with soot from an acetylene flame to reduce secondary electrons and placed 6 mm below the axis of the electron beam, incorporated into a movable source arrangement [32]. The movable gas source method has been tested previously in our laboratory and found to determine background scattering rates expediently and accurately. The range of drive pressures behind the source was about 0.07 to 0.09 Torr for THF and 0.9 to 1.1 Torr for helium. The pressure in the experimental chamber with this gas load was about 1×10^6 Torr. The gas beam temperature, determined by the apparatus temperature in the collision region, was about 65° C; however, in most of the gas handling copper tubing, the temperature was 24° C, with the higher temperature found only in the last 4 cm of the gas handling system before the gas exited into the collision region.

Based on our flow-rate vs. drive-pressure analysis [31], the gas-kinetic molecular diameter of THF was determined to be 7.57×10^{-8} cm, significantly larger than the molecular diameter quoted previously, 4.68×10^{-8} cm [15, 17]. Previously [33] we obtained a molecular diameter of 5.6×10^{-8} cm for furan, and we note here that the dipole moment of THF, 1.63 D, is larger than that of furan, 0.66 D, by a factor of 2.5 [34]; moreover, THF is more massive (molecular weight 72.11 amu, vs. 68.07 for furan) and has H atoms above and below the plane of the ring, while furan is planar. At this point we are convinced that the stated "hard sphere" diameter is incorrect when applied to molecules, such as THF, that have dominant long-range dipole-dipole interactions and inherently scatter anisotropically (mostly in the forward direction, in the center-of-mass frame), as compared to hard spheres which scatter isotropically. In Table I, we show a summary of molecular diameters δ determined from our flow measurements, which are normalized by comparison with helium ($\delta = 2.18 \times 10^{-8}$ cm) at the same temperature [35]. At low energy, the electron beam handling was made more difficult due to space-charge broadening of the beam. Careful tuning had to be undertaken

to ensure that the beam was not striking the nozzle, but also that it remained stable crossing above the nozzle.

Our elastic scattering measurements were taken at E_0 values of 0.75, 1, 1.5, 2, 3, 5, 6, 6.5, 10, 20, and 30 eV for scattering angles ranging from 10° to 130°, similar to the range covered in earlier work on water [31]. The uncertainties in the present DCS data (approximately 10% at most angles and energies) are taken to be the quadrature sum of the statistical uncertainty and reproducibility of scattered electron counts (1 to 4%), an uncertainty in the measured flow rates (5%, taken from the deviation in the gas pressure at the start and end of each measurement), and the reported uncertainty in the literature DCS values for helium (7%). The integral cross section (ICS) and momentum-transfer elastic cross section (MTCS) were computed by extrapolating the measured differential cross sections (DCSs) to 0° and 180° using theory as an aid where possible. The extrapolation at forward angles used the Born-dipole form of the DCS for a 1.63 D dipole moment and a rotational energy loss of 5 meV [4] below E_0=3.0 eV and the present calculation (see below) for higher energies. At large θ, the present calculation was used for extrapolation. The contribution to the ICS from the extrapolated Born-dipole forward peak is very large, leading to a larger error on the low-energy ICS, roughly estimated by comparing to the results of "flat-extrapolating" our DCSs to 0° and 180°. The uncertainty in the ICS estimated by comparing the flat extrapolation with the Born-dipole extrapolation ranges from about 42% at our lowest energy, 0.75 eV (where the dipolar forward peak is dominant), to about 24% at 30 eV. The uncertainty at low energies is primarily governed by the energy loss used in the Born-dipole extrapolation, which is not experimentally known. We consider 5 meV a value reasonably characteristic of rotational excitation within the elastic-scattering energy-loss peak.

B. Computational

Elastic cross sections for electrons scattering by THF were computed within the fixed-nuclei approximation using the SMC method [36, 37] as implemented for parallel computers [38]. A general description of the method may be found in the indicated references, so here we give only details specific to the present calculations. The molecular structure was taken to be the conformer having C_2 point-group symmetry, with bond lengths and angles optimized at the level of second-order Möller-Plesset perturbation theory within the 6-31G(d) basis set

using the electronic structure package GAMESS [39]. Although this is likely the minimum-energy conformer, the THF ring pseudorotates among local minima separated by small barriers [40, 41]; however, in previous work [27] we found only small differences between the cross sections obtained for C_2 and C_s tautomers.

The molecular ground-state wavefunction was described at the Hartree-Fock level within the DZV++$(2d, p)$ basis set as contained in GAMESS—that is, the double-zeta basis set of Dunning [42] with diffuse s and p orbitals on the heavy atoms, diffuse s orbitals on the hydrogens, two d polarization functions on the heavy atoms, and a polarization p orbital on the hydrogens. Default exponents and splitting factors were used for these supplemental functions. The $(x^2 + y^2 + z^2)$ linear combination of Cartesian d orbitals was excluded from the basis set. The Hartree-Fock ground state energy was -231.03449 hartree and the corresponding dipole moment 2.03 D. For comparison, the energy we obtained in the uncontracted pc-4 basis set, which should be within ~ 0.001 hartree of the Hartree-Fock limit [43], is -231.07860 hartree, and the corresponding dipole moment is 1.981 D. The experimental average dipole moment is 1.63 D [34], while the dipole moment of the minimum-energy (probably C_2) conformer is 1.75±0.02 D [40].

Electron scattering calculations were carried out using the same DZV++$(2d, p)$ basis set. We first applied an orthogonal transformation to the Hartree-Fock virtual orbitals to obtain modified virtual orbitals (MVOs) [44] using a +6 cationic Fock operator. In forming the SMC variational space, we included the 143 doublet configurations that could be formed by antisymmetrizing the neutral ground state with an MVO. To described target polarization and dynamical correlation during the collision, we further included two-particle, one-hole doublet configuration state functions formed from singlet-coupled single excitations of the ground state plus an additional MVO. In this latter set, we allowed excitations from the 5 most tightly bound valence orbitals into the 20 lowest-energy MVOs, and from the 15 outermost valence orbitals into the 30 lowest MVOs, in each case coupled with all possible MVOs. This resulted in variational spaces containing 26 027 and 26 016 configurations for the ^2A and ^2B representations of C_2, respectively. Calculations of comparable scale and using the same basis set have been found to produce good results for similarly-sized molecules such as propanol and butanol [45].

Electron scattering by a strongly polar molecule such as THF is heavily influenced by the dipole potential, particularly at forward scattering angles and at low collision energies.

Because of this potential's long range, its influence is difficult to capture fully in calculations that rely on expansions either in partial waves or, as in the SMC method, in square-integrable basis sets. Our previous results for THF [27] were not corrected for dipole-scattering effects and thus not expected to be accurate at very low energy or small angles. In the present work, we have applied the standard "Born completion" procedure [46], which in effect complements the results of a high-level calculation for low partial waves with high-partial-wave contributions computed in the first Born approximation for a point dipole potential. Our implementation of Born completion represents the amplitude $f(\vec{k}_{\rm in}), \vec{k}{\rm out})$ for scattering from initial wave vector $\vec{k}_{rmin}$ to final wave vector $\vec{k}_{\rm out}$ as

$$f(\vec{k}_{\rm in}, \vec{k}_{\rm out}) = f_{\rm Born}(\vec{k}_{\rm in}, \vec{k}_{\rm out}) + \sum_{L_{\rm out}}^{L_{\rm max}} f_{\rm SMC}(\vec{k}_{\rm in}, L_{\rm out}) - f_{\rm Born}(\vec{k}_{\rm in}, L_{\rm out}), \qquad (1)$$

where $f_{\rm SMC}$ is the result calculated with the SMC method, $f_{\rm Born}$ is the first-Born result, $L = (\ell, m)$ is a joint index for the angular momentum ℓ and its azimuthal component m, and $L_{\rm max} = (\ell_{\rm max}, \pm\ell_{\rm max})$ is the highest partial wave retained from the SMC calculation. The appropriate value of $L_{\rm max}$ depends on the incident energy E_0. Ideally, there will be a range of L values over which the SMC and first-Born partial-wave amplitudes coincide, so that any $L_{\rm max}$ within this range gives nearly the same corrected amplitude. However, at very low energies we frequently find that there is no such range of insensitivity to $L_{\rm max}$, probably because the limited spatial extent of the SMC wavefunction sets an upper limit on the angular momenta that it can represent accurately, and this upper limit decreases with decreasing collision energy. At low energies, therefore, we instead choose $L_{\rm max}$ so that the DCS at near-forward angles, which is dominated by the dipole-Born correction, joins smoothly onto the intermediate-angle DCS, which is dominated by low partial waves from the SMC calculation. In the present THF work, we used $L_{\rm max} = 1$ at 0.75 eV; $L_{\rm max} = 2$ at 1 and 1.5 eV; $L_{\rm max} = 3$ at 2 and 3 eV; $L_{\rm max} = 4$ at 5, 6, and 6.5 eV; and $L_{\rm max} = 5$, 6, and 7 at, respectively, 10, 15, and 20 eV. For E_0 around 10 eV and higher, similar results are obtained for several different values of $L_{\rm max}$, while the cutoffs at smaller E_0 are roughly consistent with $L_{\rm max} \approx \hbar R|\vec{k}|$, where R is the molecular radius.

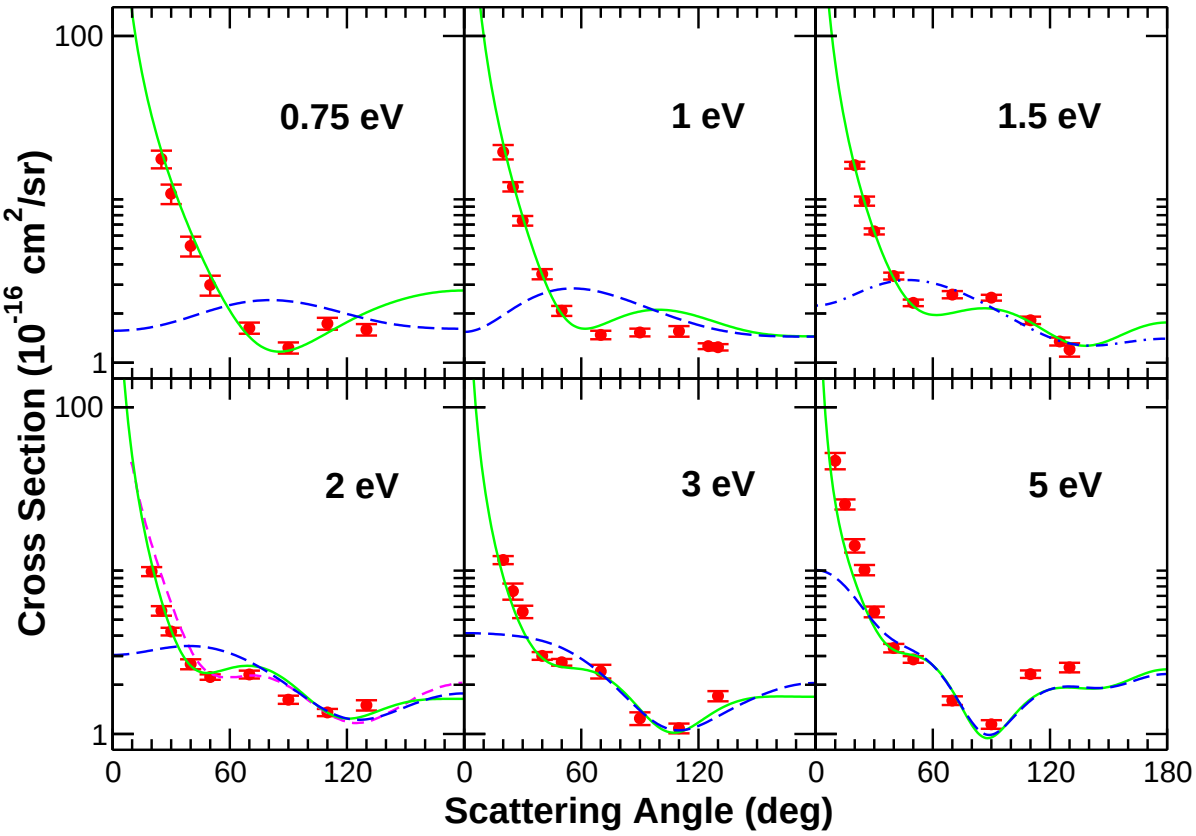

FIG. 1: (Color online) Differential cross sections for elastic electron scattering by tetrahydrofuran. The red circles are the present measured values. The solid green and dashed blue lines show the results of the present calculations with and without the Born-dipole correction. The short-dashed magenta line at 2 eV shows the measurements of Allan, Ref. [15].

III. RESULTS AND DISCUSSION

Table II lists the experimental cross sections from this work, while Figs. 1 and 2 show the present measured and calculated DCSs along with previous experimental [15–17] and theoretical [26] results. At most energies and angles, there is excellent agreement—within the quoted error bars—among the various measurements (though error bars are not shown for all data to avoid congestion). Exceptions are at 2 eV, where the results of Allan [15] are somewhat larger than the present values in the forward direction; at 10 eV, where Allan's results are somewhat smaller in the backward direction than the present results and those of Dampc *et al.;* and at 20 and 30 eV, where the various measurements agree qualitatively but

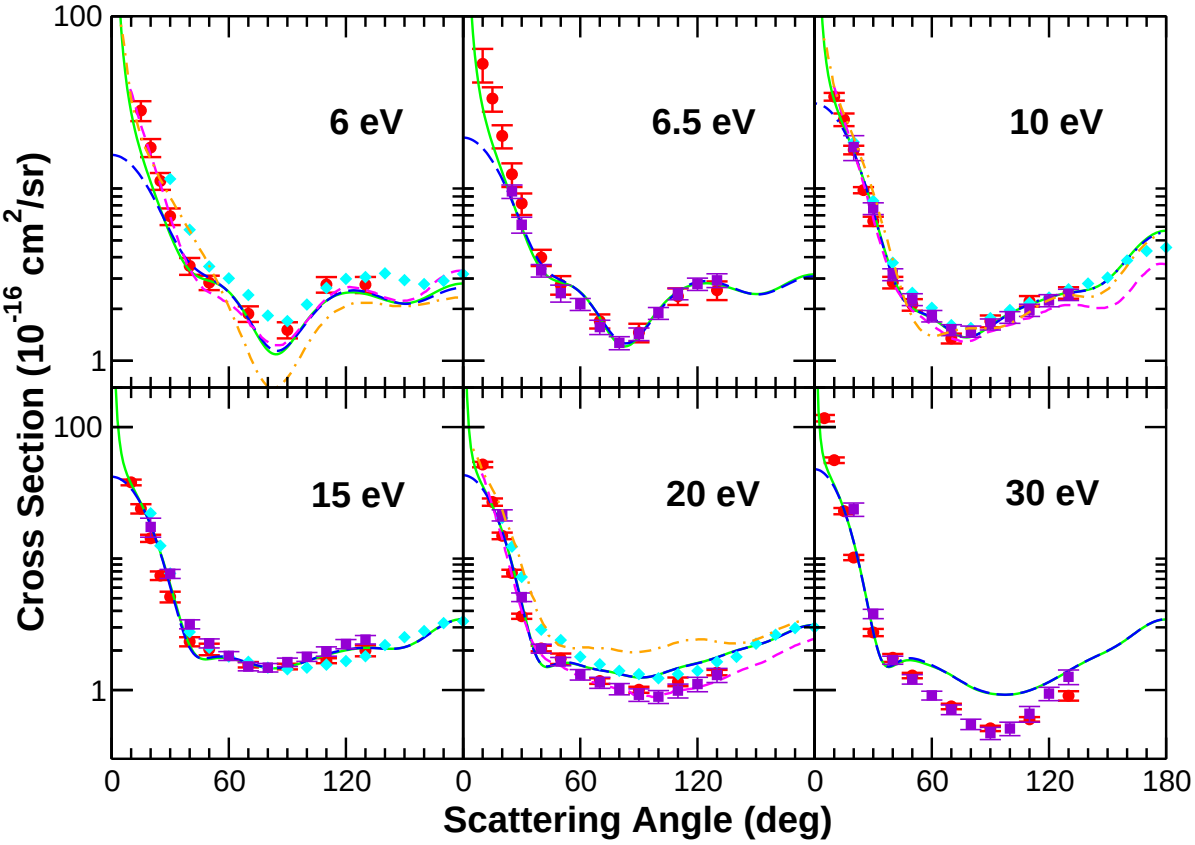

FIG. 2: (Color online) As in Fig. 1, at higher energies. Additional measured results shown are those of Colyer *et al.,* Ref. [16] (violet squares), and of Dampc *et al.,* Ref. [17] (cyan diamonds); the calculated results of Trevisan *et al.,* Ref. [26], are shown by the orange chained lines.

with more scatter in the numerical values. It is both interesting and encouraging to observe that there is generally excellent agreement between our measured values and those of Colyer *et al.* [16], even though their He/THF pressure ratio implies a much smaller hard-sphere diameter for THF, $\sim 4.8 \times 10^{-8}$ cm^2, than that which we deduce.

Agreement between the present dipole-corrected SMC results and the measured DCSs is good to excellent, depending on energy. Examination of the uncorrected SMC results, also shown in the figures, indicates that the Born-dipole correction is critical to obtaining even qualitatively correct results at the lowest energies, while at about 5 eV and above, the correction is only significant at near-forward angles. We note that single-channel calculations of the present kind tend to overestimate the DCS at higher energies and intermediate to high angles The apparent close agreement of the SMC results at 15 and 20 eV with the

data of Dampc *et al.* [17] and also with those of Milosavljević *et al.* [8] (not shown) is thus likely fortuitous, while the smaller values obtained in the present measurements are probably closer to the true DCS.

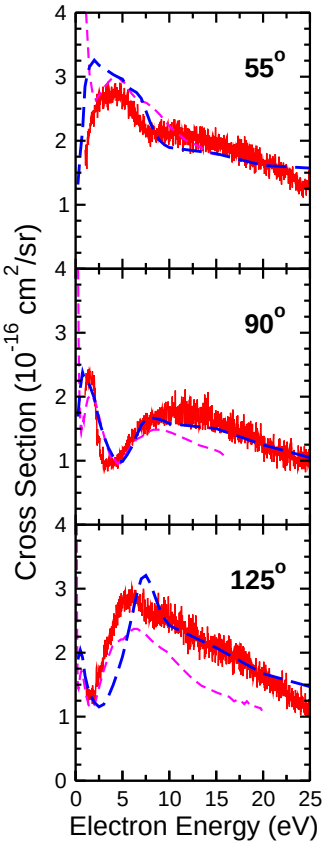

FIG. 3: (Color online) Differential cross sections for elastic electron scattering by tetrahydrofuran at fixed angles as a function of the collision energy. The present measurements are shown by the red solid line, the present calculated values (without Born-dipole correction) by the blue long-dashed line, and the measurements of Ref. [15] (at 45° in the top panel, and at 135° in the bottom panel) by the magenta short-dashed line.

DCS data collected at fixed angles as the collision energy is varied can reveal both the presence of shape resonances and possible changes in resonant behavior with scattering angle. Fig. 3 shows the elastic DCS measured in this "excitation function" mode at three scattering angles. Also shown are the present calculated results and previous data measured by Allan at the same or nearby angles [15]. Though overall agreement among the different datasets is good to excellent, some differences in detail are evident. In particular, the DCSs obtained

by Allan are smaller than the present results at larger angles and higher energies, while the calculated results at 55° and 125° differ somewhat respecting the shape and position of the peak that, in the measured data, is centered near 5 eV. Although it is tempting to interpret the peaks seen in Fig. 3 as resonances, complications must be borne in mind: not all peaks are resonant in origin, while resonances can appear not only as peaks but also as windows or other structures. Indeed, Allan [15] has suggested a nonresonant origin for the observed features.

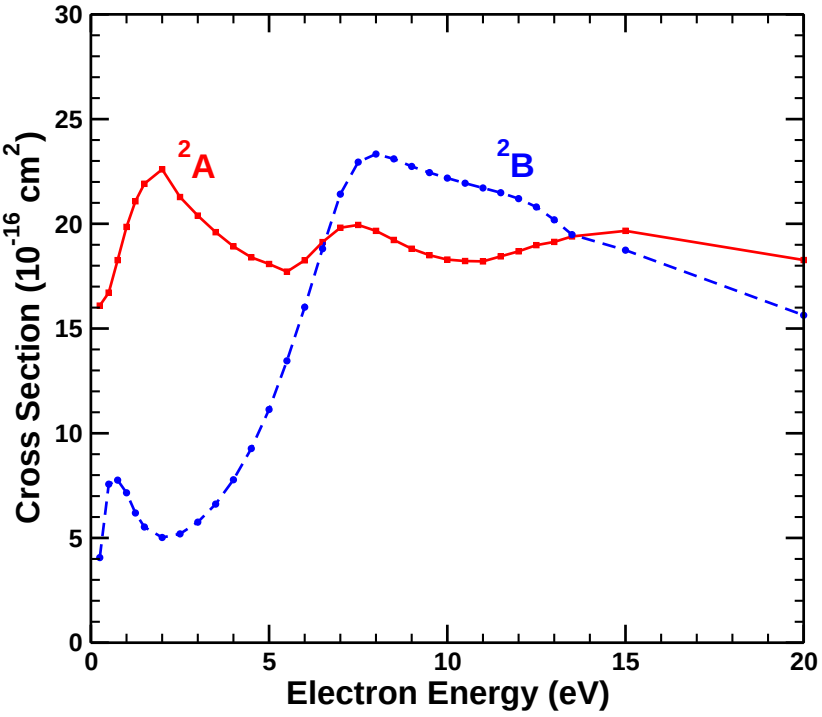

FIG. 4: (Color online) Symmetry components of the calculated integral cross section for elastic electron scattering by tetrahydrofuran, corresponding to the two irreducible representations of the C_2 point group. The Born-dipole correction for near-forward scattering is omitted from these results.

Further information about possible resonances may be gathered from Fig. 4, which shows the contributions from the ^2A and ^2B components of the SMC ICS computed in the C_2 point group. At low energy, we find maxima at about 0.75 eV in ^2B and 1.7 eV in ^2A. Similar low-energy peaks, nonresonant in origin, are seen in many other molecules, and we do not associate them with resonances in THF. On the other hand, the overlapping maxima

at about 7.5 eV (^2A) and 8.0 eV (^2B) probably do arise from shape resonances, while at still higher energies, the shoulder near 12 eV in ^2B and the broad peak around 15 eV in ^2A may also reflect short-lived shape resonances. We base these assertions in part on the corresponding eigenphase sums (not shown), which are more or less flat in the low-energy range but show broad rises in the ∼5 to 8 eV and ∼12 to 15 eV ranges. Similar results were obtained in earlier calculations. Trevisan *et al.* [26], who assumed C_{2v} symmetry for THF, found a broad peak in the ICS near 8.6 eV that arose from overlapping $^2A_1$ and $^2B_2$ resonances, while our own previous study [27] showed a peak at 8.3 eV and a shoulder at 13 to 14 eV, each arising from overlapping ^2A and ^2B features, as in the present case.

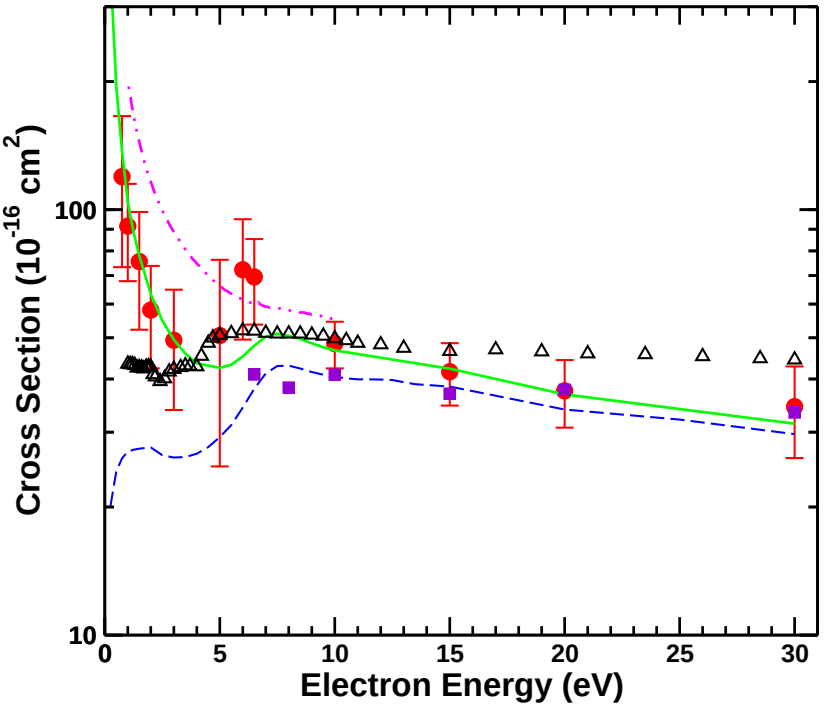

FIG. 5: (Color online) Integral cross sections for elastic electron scattering by tetrahydrofuran. Red circles are present measurements and solid green line the present calculation, both with Born-dipole correction (see text for discussion); dashed blue line is the uncorrected calculation. Previous measurements of Ref. [16] are shown by violet squares, and the previous calculation of Ref. [25] by the chained magenta line. The total scattering cross section measurements of Ref. [12] are also included for comparison (black open triangles).

Studies of electron-impact vibrational excitation of gas-phase THF have also indicated

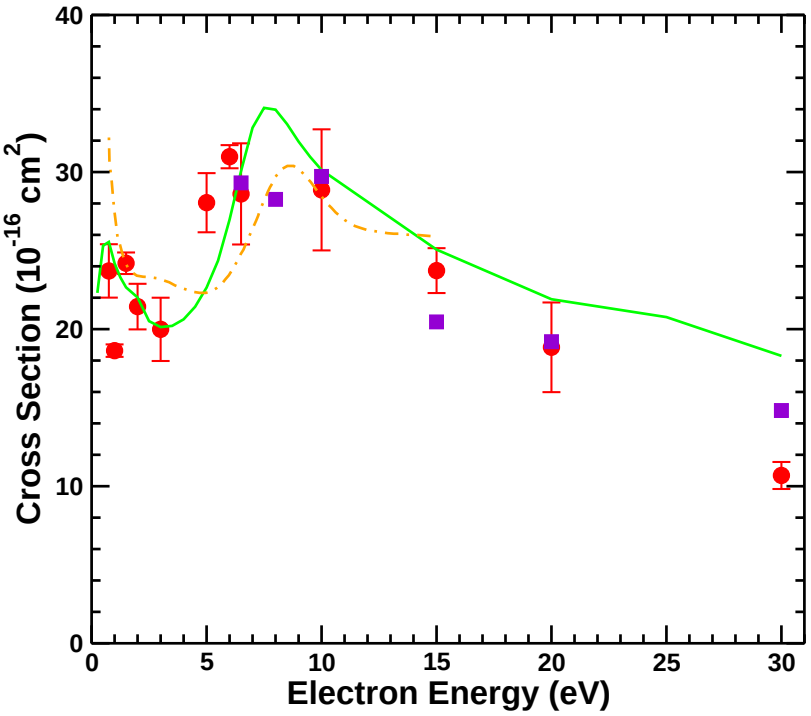

FIG. 6: (Color online) Momentum-transfer cross sections for elastic electron scattering by tetrahydrofuran. Red circles are present measurements and solid green the line present calculation, violet squares the previous measurements of Ref. [16], and orange chained line the previous calculation of Ref. [26].

the existence of shape resonances. The most recent work is that of Allan [15], which shows peaks in the excitation of several modes at 6.2 and 10.8 eV. Earlier results from Dampc *et al.* [18] showed resonant features in excitation of C–H stretching vibrations at 6.0, 7.9, and 10.3 eV, while Lepage *et al.* [4] had previously reported a peak at 8.3 eV that they interpreted as arising from a core-excited resonance. Allan notes that his results do not rule out the presence of a resonance at about 7.9 eV, which could be present but unresolved between the 6.2 and 10.8 eV features. The vibrational-excitation data suggest that the present SMC calculation places one or more resonances somewhat too high in energy; in particular, the ^2A maximum at 7.5 eV in Fig. 4 may be associated with the 6.2 eV resonance, while the ^2B shoulder near 12 eV may be associated with the 10.8 eV resonance. The fixed-angle DCS results at 125° (Fig. 3) also suggest the first ^2A resonance may be placed too high. Previous calculations [26, 27] with more limited treatments of polarization gave even higher resonance

energies.

The integral and momentum-transfer cross sections derived from the present DCSs are shown in Figs. 5 and 6, respectively, along with selected results from previous work. We note that the fixed-nuclei elastic ICS for a polar molecule is technically divergent. The Born-dipole corrected values of the SMC ICS shown in Fig. 5 are obtained not by considering rotational inelasticity to make the forward DCS finite but simply by starting the integration of the corrected DCS at 0.1° rather than 0°. The present measured and calculated results for the ICS agree well with each other and with the previous measurements of Colyer *et al.* [16]. In most cases, moreover, they are consistent with (that is, smaller than) the total cross section (TCS) reported by Możejko *et al.* [12] within the combined error bars, the exception being at energies of 3 eV and lower, where the TCS does not exhibit the increase expected in a polar molecule such as THF, perhaps indicating a failure to discriminate sufficiently between unscattered electrons and those scattered through a very small angle. The various MTCS results shown in Fig. 6 generally agree well, though the differences in resonance positions discussed above are evident. Our calculated MTCS in Fig. 6 omits the Born-dipole correction because the factor of $(1-\cos\theta)$ makes forward scattering much less important to the MTCS than the ICS.

To summarize, the present results show that excellent agreement between measured and calculated differential cross sections for electron scattering by THF can be obtained even at collision energies as low as 1 eV, but only if long-range scattering from the dipole potential is included in the calculation. Both results obtained at fixed angles as a function of energy and angle-integrated results reflect the existence of several shape resonances, and the present calculations do a better, but still not fully satisfactory, job of predicting the resonance energies than prior calculations. However, neither the measured nor the calculated results indicate the existence of shape resonances in the 0 to 5 eV range that could be implicated in dissociative attachment to THF. This result is consistent with the weak dissociative attachment in fact observed in THF [10] and supports the hypothesis that the processes responsible for DNA strand breaking by low-energy electrons involve initial attachment elsewhere, most likely on the nucleobases.

Acknowledgments

This work was sponsored by the U.S. National Science Foundation under Grants PHY 0653452 (M.A.K.) and PHY 0653396 (V.M. and C.W.). The work of V.M. and C.W. was supported by the Chemical Sciences, Geosciences and Biosciences Divsion, Office of Basic Energy Sciences, Office of Science, U.S. Department of Energy, and made use of the Jet Propulsion Laboratory's Supercomputing and Visualization Facility.

---

[1] B. Boudaïffa, P. Cloutier, D. Hunting, M. A. Huels, and L. Sanche, Science **287**, 1658 (2000).

[2] M. A. Huels, B. Boudaïffa, P. Cloutier, D. Hunting, and L. Sanche, J. Am. Chem. Soc. **125**, 4467 (2003).

[3] L. J. Bremner, M. G. Curtis, and I. C. Walker, J. Chem. Soc. Faraday Trans. **87**, 1049 (1991).

[4] M. Lepage, S. Letarte, M. Michaud, F. Motte-Tollet, M.-J. Hubin-Franskin, D. Roy, and L. Sanche, J. Chem. Phys. **109**, 5980 (1998).

[5] D. Antic, L. Parenteau, M. Lepage, and L. Sanche, J. Phys. Chem. B **103**, 6611 (1999).

[6] D. Antic, L. Parenteau, and L. Sanche, J. Phys. Chem. B **104**, 4711 (2000).

[7] S.-P. Breton, M. Michaud, C. Jäggle, P. Swiderek, and L. Sanche, J. Chem. Phys. **121**, 11240 (2004).

[8] A. R. Milosavljević, A. Giuliani, D. Šević, M.-J. Hubin-Franskin, and B. P. Marinković, Eur. Phys. J. D **35**, 411 (2005).

[9] A. Zecca, C. Perazzolli, and M. J. Brunger, J. Phys. B **38**, 2079 (2005).

[10] K. Aflatooni, A. M. Scheer, and P. D. Burrow, J. Chem. Phys. **125**, 054301 (2006).

[11] C. Jäggle, P. Swiderek, S.-P. Breton, M. Michaud, and L. Sanche, J. Phys. Chem. B **110**, 12512 (2006).

[12] P. Możejko, E. Ptaskińska-Denga, A. Domaracka, and Cz. Szmytkowski, Phys. Rev. A **74**, 012708 (2006).

[13] Y. S. Park, H. Cho, L. Parenteau, A. D. Bass, and L. Sanche, J. Chem. Phys. **125**, 074714 (2006).

[14] P. Sulzer, S. Ptasinska, F. Zappa, B. Mielewska, A. R. Milosavljevic, P. Scheier, T. D. Märk, I. Bald, S. Gohlke, M. A. Huels, and E. Illenberger, J. Chem. Phys. **125**, 044304 (2006).

[15] M. Allan, J. Phys. B **40**, 3531 (2007).

[16] C. J. Colyer, V. Vizcaino, J. P. Sullivan, M. J. Brunger, and S. J. Buckman, New J. Phys. **9**, 41 (2007).

[17] M. Dampc, A. Milosavljević, I. Linert, B. P. Marinković, and M. Zubek, Phys. Rev. A **75**, 042710 (2007).

[18] M. Dampc, I. Linert, A. R. Milosavljević, and M. Zubek, Chem. Phys. Lett. **443**, 17 (2007).

[19] B. C. Ibănescu, O. May, and M. Allan, Phys. Chem. Chem. Phys. **10**, 1507 (2008).

[20] A. Milosavljević, D. Šević, and B. P. Marinković, J. Phys. Conf. Ser. **101**, 012014 (2008).

[21] M. Fuss, A. Muñoz, J. C. Oller, F. Blanco, D. Almeida, P. Limão-Vieira, T. P. D. Do, M. J. Brunger, and G. García, Phys. Rev. A **80**, 052709 (2009).

[22] A. Giuliani, P. Limão-Vieira, D. Duflot, A. R. Milosavljevic, B. P. Marinkovic, S. V. Hoffmann, N. Mason, J. Delwiche, and M.-J. Hubin-Franskin, Eur. Phys. J. D **51**, 97 (2009).

[23] T. P. T. Do, M. Leung, M. Fuss, G. Garcia, F. Blanco, K. Ratnavelu, and M. J. Brunger, J. Chem. Phys. **134**, 144302 (2011).

[24] P. Możejko and L. Sanche, Radiat. Phys. Chem. **73**, 77 (2005).

[25] D. Bouchiha, J. D. Gorfinkiel, L. G. Caron, and L. Sanche, J. Phys. B **39**, 975 (2006).

[26] C. N. Trevisan, A. E. Orel, and T. N. Rescigno, J. Phys. B **39**, L255 (2006).

[27] C. Winstead and V. McKoy, J. Chem. Phys. **125**, 074302 (2006).

[28] S. Tonzani and C. H. Greene, J. Chem. Phys. **125**, 094504 (2006).

[29] M. A. Khakoo, C. E. Beckmann, S. Trajmar, and G. Csanak, J. Phys. B **27**, 3159 (1994).

[30] J. H. Brunt, G. C. King, and F. H. Read, J. Phys. B **10**, 1289 (1977).

[31] M. A. Khakoo, H. Silva, J. Muse, M. C. A. Lopes, C. Winstead, and V. McKoy, Phys. Rev. A **78**, 052710 (2008).

[32] M. Hughes, K. E. James, Jr., J. G. Childers, and M. A. Khakoo, Meas. Sci. Technol. **14**, 841 (1994).

[33] M. A. Khakoo, J. Muse, K. Ralphs, R. F. da Costa, M. H. F. Bettega, and M. A. P. Lima, Phys. Rev. A **81**, 062716 (2010).

[34] R. C. Weast, ed., *CRC Handbook of Chemistry and Physics*, 58th Ed. (CRC Press, Boca Raton, 1978), p. E-65.

[35] S. Dushman and J. M. Lafferty, *The Scientific Foundations of Vacuum Technique*, 2nd ed. (John Wiley and Sons, New York, 1962).

[36] K. Takatsuka and V. McKoy, Phys. Rev. A **24**, 2473 (1981).

[37] K. Takatsuka and V. McKoy, Phys. Rev. A **30**, 1734 (1984).

[38] C. Winstead and V. McKoy, Comput. Phys. Commun. **128**, 386 (2000).

[39] M. W. Schmidt, K. K. Baldridge, J. A. Boatz, S. T. Elbert, M. S. Gordon, J. H. Jensen, S. Koseki, N. Matsunaga, K. A. Nguyen, S. J. Su, T. L. Windus, M. Dupuis, and J. A. Montgomery, J. Comput. Chem. **14**, 1347 (1993).

[40] G. G. Engerholm, A. C. Luntz, W. D. Gwinn, and D. O. Harris, J. Chem. Phys. **50**, 2446 (1969).

[41] V. M. Rayón and J. A. Sordo, J. Chem. Phys. **122**, 204303 (2005).

[42] T.H. Dunning, Jr., and P. J. Hay, in *Methods of Electronic Structure Theory,* H. F. Schaefer III, ed. (Plenum, New York, 1977), p. 1.

[43] F. Jensen, Theor. Chem. Acc. **113**, 267 (2005).

[44] C. W. Bauschlicher, J. Chem. Phys. **72**, 880 (1980).

[45] M. A. Khakoo, J. Muse, H. Silva, M. C. A. Lopes, C. Winstead, V. McKoy, E. M. de Oliveira, R. F. da Costa, M. T. do N. Varella, M. H. F. Bettega, and M. A. P. Lima, Phys. Rev. A **78**, 062714 (2008).

[46] T. N. Rescigno and B. I. Schneider, Phys. Rev. A **45**, 2894 (1992), and references therein.

TABLE II: Differential cross sections and error estimates (10^{-16} cm^2/sr) for elastic electron scattering by tetrahydrofuran. Integral cross sections $\sigma_{\rm I}$, momentum-transfer cross sections $\sigma_{\rm MT}$, and corresponding error estimates (10^{-16} cm^2) are shown at the foot of each column. Extrapolated DCS values used to determine σ_I and σ_{MT} are shown in italics. The notation (n) signifies $\times 10^n$.

Angle	Energy (eV)																					
(deg)	0.75		1		2		3		5		6		6.5		10		15		20		30	
0	*2.45(6)*		*3.26(6)*		*4.90(6)*		*1.23(6)*		*9.53(5)*		*5.03(5)*		*3.36(5)*		*2.94(5)*		*1.06(5)*		*7.07(4)*		*7.95(4)*		*1.13(3)*	
1	*9.12(3)*		*6.85(3)*		*4.57(3)*		*3.43(3)*		*3.53(3)*		*4.37(3)*		*3.38(3)*		*2.96(3)*		*1.09(3)*		*743*		*852*		*1.13(3)*	
5	*366*		*275*		*183*		*137*		*142*		*155*		*156*		*144*		*67.1*		*63.1*		*85.8*		116	11
10	*91.8*		*68.8*		*45.9*		*34.4*		*35.8*		47.1	6.6	52.7		52.9	11.7	34.1	3.5	38.0	3.6	51.9	4.8	55.7	5.2
15	*40.9*		*30.7*		*20.5*		*15.3*		17.5	4.0	25.5	2.7	28.4	2.7	33.3	5.4	25.1	3.5	24.0	2.7	26.9	2.8	22.8	2.2
20	*23.1*		19.5	2.5	16.2	1.5	9.88	1.01	11.6	1.1	14.2	1.8	17.3	1.6	20.2	3.1	16.8	2.4	14.3	1.5	15.0	1.5	10.1	0.9
25	17.7	2.6	11.9	1.2	9.77	1.00	5.68	0.59	7.48	1.05	10.1	1.1	11.1	0.8	12.1	1.9	9.79	0.97	7.42	0.81	7.74	0.77		
30	10.8	1.7	7.40	0.78	6.37	0.58	4.24	0.41	5.54	0.66	5.60	0.62	6.90	0.53	8.19	1.17	6.46	0.91	5.11	0.63	3.62	0.33	2.69	0.27
40	5.19	0.83	3.49	0.37	3.39	0.32	2.68	0.28	2.99	0.29	3.36	0.33	3.55	0.29	3.98	0.43	2.85	0.43	2.34	0.26	2.06	0.19	1.71	0.18
50	2.99	0.48	2.08	0.22	2.33	0.21	2.23	0.20	2.69	0.25	2.86	0.27	2.84	0.15	2.76	0.34	2.12	0.28	2.05	0.26	1.71	0.21	1.26	0.12
70	1.63	0.18	1.48	0.15	2.61	0.25	2.31	0.22	2.39	0.30	1.60	0.16	1.88	0.11	1.70	0.16	1.35	0.14	1.56	0.15	1.16	0.11	0.718	0.067
90	1.23	0.14	1.53	0.15	2.50	0.23	1.62	0.16	1.18	0.14	1.15	0.12	1.51	0.10	1.46	0.18	1.70	0.25	1.51	0.14	1.00	0.10	0.479	0.045
110	1.74	0.20	1.56	0.17	1.82	0.17	1.35	0.13	1.07	0.11	2.33	0.22	2.77	0.18	2.37	0.26	2.22	0.29	1.67	0.15	1.12	0.13	0.565	0.050
125			1.26	0.11	1.35	0.13																		
130	1.59	0.18	1.24	0.11	1.20	0.15	1.50	0.16	1.69	0.18	2.56	0.27	2.77	0.18	2.57	0.32	2.48	0.30	2.00	0.25	1.36	0.13	0.875	0.101
140	*1.81*		*1.13*		*1.20*		*1.58*		*1.90*		*2.47*		*2.48*		*2.32*		*2.59*		*1.92*		*1.50*		*1.00*	
150	*1.98*		*1.06*		*1.03*		*1.72*		*2.01*		*2.52*		*2.37*		*2.20*		*2.95*		*1.97*		*1.64*		*1.10*	
160	*2.11*		*1.03*		*1.06*		*1.79*		*2.04*		*2.77*		*2.54*		*2.34*		*3.91*		*2.35*		*1.86*		*1.24*	
170	*2.19*		*1.02*		*1.03*		*1.80*		*2.03*		*3.08*		*2.90*		*2.68*		*5.12*		*2.93*		*2.18*		*1.45*	
180	*2.21*		*1.01*		*1.03*		*1.80*		*2.03*		*3.24*		*3.09*		*2.86*		*5.69*		*3.22*		*2.34*		*1.56*	
$\sigma_{\rm I}$	142	59	91.6	31.3	88.8	30.2	58.1	19.9	60.9	24.6	72.1	25.1	72.2	21.5	69.5	18.3	49.3	12.4	41.6	7.0	37.5	6.8	34.4	8.4
$\sigma_{\rm MT}$	23.7	4.0	18.6	2.4	22.7	3.0	21.5	2.8	21.5	3.5	28.2	3.8	31.0	3.4	28.6	5.0	30.5	3.9	23.7	3.2	18.8	2.4	10.7	1.3